HHS Public Access

Author manuscript

Cancer Cell. Author manuscript; available in PMC 2016 July 13.

Published in final edited form as:

Cancer Cell. 2015 July 13; 28(1): 70–81. doi:10.1016/j.ccell.2015.05.010.

PF-06463922, an ALK/ROS1 inhibitor, overcomes resistance to 1st and 2nd generation ALK inhibitors in pre-clinical models

Helen Y. Zou[1,5], **Luc Friboulet**[2,5], **David P. Kodack**[3,5], **Lars D. Engstrom**[1], **Qiuhua Li**[1], **Melissa West**[1], **Ruth W. Tang**[1], **Hui Wang**[1], **Konstantinos Tsaparikos**[1], **Jinwei Wang**[1], **Sergei Timofeevski**[1], **Ryohei Katayama**[4], **Dac M. Dinh**[1], **Hieu Lam**[1], **Justine L. Lam**[1], **Shinji Yamazaki**[1], **Wenyue Hu**[1], **Bhushankumar Patel**[3], **Divya Bezwada**[3], **Rosa L. Frias**[2], **Eugene Lifshits**[2], **Sidra Mahmood**[2], **Justin F. Gainor**[2], **Timothy Affolter**[1], **Patrick B. Lappin**[1], **Hovhannes Gukasyan**[1], **Nathan Lee**[1], **Shibing Deng**[1], **Rakesh K Jain**[3], **Ted W. Johnson**[1], **Alice T. Shaw**[2], **Valeria R. Fantin**[1], and **Tod Smeal**[1,*]

[1]Pfizer World Wide Research and Development, 10724 Science Center Drive, Sand Diego, California 92121

[2]Massachusetts General Hospital Cancer Center, Department of Medicine, Harvard Medical School, Boston, Massachusetts

[3]Edwin L. Steele Laboratory, Department of Radiation Oncology, Massachusetts General Hospital, Harvard Medical School, Boston, Massachusetts

[4]Cancer Chemotherapy Center, Japanese Foundation for Cancer Research, Tokyo, Japan

SUMMARY

We report the preclinical evaluation of PF-06463922, a potent and brain penetrant ALK/ROS1 inhibitor. Compared to other clinically available ALK inhibitors, PF-06463922 displayed superior potency against all known clinically acquired ALK mutations, including the highly resistant G1202R mutant. Furthermore, PF-06463922 treatment led to regression of EML4-ALK driven brain metastases, leading to prolonged mouse survival, in a superior manner. Finally, PF-06463922 demonstrated high selectivity and safety margins in a variety of preclinical studies. These results suggest that PF-06463922 will be highly effective for the treatment of patients with ALK-driven lung cancers, including those who relapsed on clinically available ALK inhibitors due to secondary ALK kinase domain mutations and/or due to the failed control of brain metastases.

[*]To whom correspondence should be addressed: Tod Smeal, Oncology Research Unit, Pfizer World Wide Research & Development, 10724 Science Center Drive, San Diego, CA 92121, Telephone: (858) 622-8081, tod.smeal@pfizer.com.

[5]H. Zou, L. Friboulet, and D. Kodack contributed equally to this work.

AUTHOR CONTRIBUTIONS

H.Y.Z., L.F., and D.P.K. contributed to the conception and design of this study, to the acquisition of data, to the analysis and interpretation of data and to the writing of the manuscript. H.Y.Z. primarily focused on the H3122 and engineered cell lines on in vitro and in vivo target inhibition and efficacy, PKPD relationships in subcutaneous and brain xenograft models. L.F. focused primarily on patient derived cell line studies including the biochemical analysis. D.P.K. mainly focused on the brain metastasis studies.

INTRODUCTION

The clinical success of targeting oncogenic tyrosine kinases that are genetically altered through activating mutations, gene translocations, or gene amplification has launched a new era of cancer therapy (Weinstein, 2002). However, acquired resistance is a major limitation to the efficacy of tyrosine kinase inhibitors (TKIs) in the clinic (Bagrodia et al., 2012; Lackner et al., 2012; Rosenzweig, 2012). Crizotinib, a small molecule inhibitor of the MET, ALK and ROS1 tyrosine kinases, is highly active in lung cancers harboring chromosomal rearrangements of ALK or ROS1. In ALK-positive NSCLC patients, crizotinib demonstrated an objective response rate of about 60% and a median progression free survival of approximately 8 to 11 months (Camidge et al., 2012; Gerber and Minna, 2010; Kwak et al., 2010; Shaw et al., 2013; Solomon et al., 2014c). Similar to the experience with other TKIs, several resistance mechanisms have been observed in patients who relapse on crizotinib. These resistance mechanisms include secondary ALK kinase domain mutations (Choi et al., 2010; Doebele et al., 2012; Katayama et al., 2011; Katayama et al., 2012; Sasaki et al., 2011), ALK gene amplification (Doebele et al., 2012; Katayama et al., 2012; Kim et al., 2013), bypass downstream signaling via EGFR (Katayama et al., 2012; Sasaki et al., 2011; Tanizaki et al., 2012), KIT (Katayama et al., 2012), SRC (Crystal et al., 2014) or IGF-1R (Lovly et al., 2014), and pharmacological resistance due to sub-optimal central nervous system (CNS) exposure (Costa et al., 2011; Gandhi et al., 2013; Maillet et al., 2013; Weickhardt et al., 2012). Roughly 30% of crizotinib refractory tumors have been shown to harbor resistance mutations in the ALK kinase domain, including G1269A, L1196M, C1156Y, L1152R, S1206Y, 1151Tins, G1202R and F1174L (Gainor and Shaw, 2013). While crizotinib has shown clinical activity against brain metastases (Costa et al., 2013; Kaneda et al., 2013; Kinoshita et al., 2013; Takeda et al., 2013), progression in the brain is particularly common in relapsed patients (Costa et al., 2015; Weickhardt et al., 2012).

Recently, the 2nd generation ALK inhibitors ceritinib and alectinib have been approved for use in crizotinib-relapsed ALK-positive NSCLC patients in the U.S., and for ALK-positive crizotinibnaive NSCLC patients in Japan, respectively (Chen et al., 2013; Gadgeel et al., 2014; Kinoshita et al., 2012; Shaw et al., 2014a). While both ALK inhibitors show efficacy in these settings, resistance to both of these inhibitors has emerged. In the case of ceritinib, relapsed tumors often express the ALK mutant G1202R (Friboulet et al., 2014). In the case of alectinib, in addition to G1202R, two ALK resistance mutations (V1180L and I1171T) have been observed (Ignatius Ou et al., 2014; Katayama et al., 2014). Some ALK mutants such as G1202R confer high-level resistance to all clinically available ALK inhibitors (Friboulet et al., 2014; Ignatius Ou et al., 2014; Shaw and Engelman, 2013). Both ceritinib and alectinib have demonstrated activity in brain metastases of crizotinib-relapsed patients. A phase 1/2 clinical trial of alectinib showed a CNS response rate of 52% (Gadgeel et al., 2014). Despite the observed CNS activity with these agents, it remains common for patients to relapse with CNS progression. A full understanding of the activity of clinically available ALK inhibitors on brain metastases is still emerging, and we provide a glimpse into mechanisms for their resistance here.

We initiated a drug discovery program with the goal of developing a next generation ALK inhibitor that is more potent and selective than other known ALK inhibitors (including

current 2nd generation inhibitors), capable of inhibiting all known resistant ALK mutants and able to penetrate the blood-brain barrier (BBB) to achieve therapeutic CNS drug concentrations. PF-06463922, an ATP-competitive small molecule inhibitor of ALK/ROS1, was successfully discovered by the optimization of physicochemical properties guided by structure based drug design (Johnson et al., 2014). Here we investigate the preclinical antitumor activity of PF- 06463922 in both subcutaneous and intracranial tumor models.

RESULTS

PF-06463922 has sub-nanomolar biochemical and nanomolar cellular potency against wildtype and crizotinib-resistant ALK mutants

PF-06463922 is a potent, reversible, ATP-competitive inhibitor of recombinant ALK kinase (Fig. S1A). In biochemical assays, PF-06463922 inhibited the catalytic activity of recombinant human wild-type ALK with a mean Ki of <0.07 nM (Fig. 1A). In addition, PF-06463922 showed a range of mean Ki values of <0.1 nM to 0.9 nM against the following crizotinib-resistant ALK mutants: L1196M, G1269A, 1151Tins, F1174L, C1156Y, L1152R, and S1206Y. PF-06463922 was more potent than crizotinib, ceritinib and alectinib against wild type ALK in biochemical studies (Fig. 1B). In addition to its high potency against ALK, PF-06463922 has previously demonstrated sub-nanomolar cell potency against ROS1 (Zou et al., 2015) and demonstrated >100-fold selectivity vs. non-target kinases, relative to the ALK^{L1196M} gatekeeper mutant, for >95% of the 206 kinases tested (Johnson et al., 2014).

To directly compare the potencies of PF-06463922, crizotinib, ceritinib and alectinib in cell assays, NIH3T3 and Ba/F3 cells were engineered to express either wild-type or the crizotinib-resistant mutants 1151Tins, L1152R, C1156Y, L1196M, G1269A, G1202R, F1174L, or S1206Y (Fig. 1C, Fig. S1B and Table S1). We observed a strong correlation between drug concentrations required to inhibit ALK phosphorylation and those needed to block ALK dependent cell proliferation (Fig. 1C). PF-06463922 was the most potent inhibitor against all clinically relevant crizotinib-, certinib- and/or alectinib-resistant ALK mutants. PF-06463922 showed strong ALK phosphorylation potency against the L1196M (IC_{50} = 15–43 nM) and G1269A (IC_{50} = 14–80 nM) ALK mutants, which are two of the most frequently detected crizotinib-resistant mutations observed in the clinic (Doebele et al., 2012; Kim et al., 2013). Furthermore, PF-06463922 demonstrated potent ALK phosphorylation activity against the 1151Tins (IC_{50} = 38–50 nM) and G1202R (IC_{50} = 77–113 nM) ALK mutants that confer a high-level of resistance to all 2nd generation ALK inhibitors (Katayama et al., 2012; Shaw and Engelman, 2013).

PF-06463922 inhibits ALK-dependent cell growth in vitro

The activity of PF-06463922 on cell viability and intracellular signaling was examined in H3122 and H2228 ALK-positive lung cancer cell lines. In addition, we examined H3122 cells engineered to overexpress the crizotinib-resistant ALK mutants, G1269A or L1196M. Similar to the Ba/F3 cell model, in these cell lines PF-06463922 was greater than 30-fold more potent than crizotinib with respect to suppressing ALK-dependent signaling and inhibiting cell growth and inducing apoptosis (Fig. 2A–E Fig. S2A–D and Table S1).

Furthermore, the cell viability of in vitro-derived alectinib-resistant H3122 cells, which contain an endogenous V1180L ALK mutation (Katayama et al., 2014), was sensitive to PF-06463922 via potent inhibition of ALK signaling (Fig. 2F and S2E).

The efficacy of PF-06463922 was also examined in cell lines derived from patients with acquired resistance to crizotinib, ceritinib or alectinib. These cells lines, SNU2535, MGH021-5 and MGH056-1, harbor endogenous EML4-ALK^{G1269A}, SQSTM1-ALK^{G1202R} or EML4-ALK^{I1171T} mutations, respectively. PF-06463922 exhibited significantly greater cell growth inhibitory potency in these cell lines compared to crizotinib. Cell growth IC_{50} values for PF-06463922 were 47 nM, 63 nM and 23 nM, respectively, compared with 3240 nM, 1046 nM and 271 nM, respectively, for crizotinib (Fig. 2G–I). These cell growth IC_{50} values correlated closely with the drugs' abilities to inhibit ALK phosphorylation and downstream signaling in these cells (FS2F–H). Overall, in both the patient-derived and engineered cell lines, PF-06463922 consistently showed greater potency in inhibiting ALK phosphorylation and cell viability compared to clinically available ALK inhibitors.

PF-06463922 exhibits potent antitumor efficacy in vivo, and its pharmacokinetic-pharmacodynamic relationship in these models

PF-06463922 was evaluated for its efficacy against subcutaneous (S.C.) growth of parental H3122 EML4-ALK^{WT} and engineered H3122 EML4-ALK^{L1196M}, EML4-ALK^{G1269A} and NIH- 3T3 EML4-ALK^{G1202R} tumors (Fig. 3A–D). In these experiments, PF-06463922 was administered by subcutaneous pump infusion, which better mimics the predicted human PK profile than oral dosing in mice (data not shown). Treatment with PF-06463922 led to a dose-dependent antitumor effect ranging from tumor growth inhibition (TGI) to tumor regression. The effect on tumor growth was consistent with its ability to dose-dependently inhibit ALK phosphorylation. A maximal effect (Emax) of > 95% inhibition of ALK phosphorylation was achieved in each of the models, and this resulted in tumor regression ranging from 35% to 77% (Fig. 3 and Table S2). Of note, PF-06463922 significantly inhibited tumor growth in crizotinib-resistant models harboring mutant ALK, including the most resistant G1202R mutant.

A simple direct response pharmacokinetic (PK)-pharmacodynamic (PD) modeling analysis (Mager et al., 2003) was conducted to elucidate the relationship between PF-06463922 plasma concentration, inhibition of ALK phosphorylation and suppression of tumor growth. The Hill equation showed reasonable fits for both inhibition of ALK phosphorylation and antitumor efficacy (Fig. S3A–S3D). The PK, PD, TGI and Hill equation parameters of PF-06463922 from these studies are summarized in Tables S2 and S3, and the efficacious concentrations (Ceff) derived from the Hill function analyses are summarized in Table S4. To summarize, the Ceffs for tumor stasis (100% TGI) were determined to be 6.5 nM in the H3122 EML4-ALK^{WT} tumor model, 38 nM in the H3122 EML4-ALK^{G1269A} model, 68 nM in the H3122 EML4-ALK^{L1196M} model and 165 nM in the 3T3 EML4-ALK^{G1202R} model. The estimated effective concentrations (EC50) for inhibiting ALK phosphorylation were comparable to the Ceff values for tumor stasis of each corresponding ALK fusion (Table S4). The Ceff (68 nM free) determined for the H3122 EML4-ALK^{L1196M} model with PF-06463922 administered by infusion is similar to the Ceff (51 nM free) determined using

the oral route (Yamazaki et al., 2014). The Ceffs for maximum antitumor response for PF-06463922 correlated closely with the estimated EC_{90} values for ALK phosphorylation inhibition in these tumors (Fig. S3A–S3D and Table S4).

An oral dosing study in the H3122-EML4-ALK^{L1196M} model demonstrated significant tumor regression (35%) and greater than 95% inhibition of ALK phosphorylation in the 10 mg/kg/day BID group. The antitumor efficacy of the 10 mg/kg/day BID oral dosing schedule was similar to that of the 30 mg/kg/day QD group (33% regression), and superior to the 10 mg/kg/day QD group (3% tumor regression) (Fig. S3E). The 10 mg/kg/day BID group had lower unbound plasma Cmax (maximal plasma concentration) (392 nM) than either the 10 mg/kg/day QD (1,636 nM) or the 30 mg/kg/day QD (3,193 nM) groups, indicating that the antitumor efficacy of PF06463922 was not driven by Cmax in this model (Table S2). Collectively, these results indicate that near complete inhibition of ALK phosphorylation (> 95%) with prolonged duration during the dosing interval by PF-06463922 is necessary to achieve maximal tumor regression, and PF-06463922 is able to achieve this activity at a relatively low dose.

PF-06463922 drives superior tumor growth inhibition in vivo compared to crizotinib

The in vivo efficacy of PF-06463922 was directly compared to crizotinib in engineered H3122 models and patient-derived cell lines. Consistent with in vitro data, PF-06463922 showed superior efficacy compared to crizotinib in tumor xenografts derived from H3122 EML4-ALK^{WT} (Fig. S4A), H3122 EML4-ALK^{L1196M} (Fig. 4A) and H3122 EML4-ALK^{G1269A} cells (Fig. S4B). In parallel with tumor growth, PF-06463922 inhibited ALK-mediated signal transduction in tumor tissues collected 3 hours following the final dose of a 4-day treatment regimen to a greater extent than crizotinib. Specifically, ALK, AKT, ERK, STAT3 and S6 phosphorylation were significantly decreased by PF-06463922 in the respective H3122 EML4-ALK models (Fig. S4C D and E). This data corresponded to dose-dependent induction of cleaved caspase 3 levels measured in H3122 EML4-ALK^{L1196M} tumor samples from mice treated with 3 and 10 mg/kg/day of PF-06463922 (Fig. 4B). Of note, in H3122 EML4-ALK^{WT} tumor bearing mice, PF-06463922 showed similar efficacy in inhibiting tumor growth and ALK phosphorylation compared to alectinib (Fig. S4A and S4C).

Two ALK-positive patient derived cell lines were also used to evaluate the *in vivo* antitumor efficacy of PF-06463922 against wild type EML4-ALK. MGH051 (EML4-ALK^{WT}) (Fig. 4C) was derived from a crizotinib-resistant ALK-positive NSCLC patient (Friboulet et al., 2014). MGH006 (EML4-ALK^{WT}) (Fig. S4F) was derived from a crizotinib-naive ALK-positive NSCLC patient (Katayama et al., 2012). Oral administration of PF-06463922 potently suppressed ALK phosphorylation and led to substantial tumor regression of these xenograft models (Fig. S4G and H).

The antitumor efficacy of PF-06463922 in xenograft models was durable. PF-06463922 suppressed subcutaneous tumor growth longer than 170 days in both MGH051 (EML4-ALK^{WT}) (Fig. 4C) and H3122-EML4-ALK^{G1269A} (Fig. 4D) and models at drug concentrations predicted to be clinically achievable. Moreover, PF-06463922 induced tumor regression in mice bearing MGH051 tumors that relapsed on crizotinib (Fig. 4C).

PF-06463922 induced superior regression of intracranial EML4-ALK tumors and prolonged mouse survival compared to other clinically-available ALK inhibitors

Nearly 50% of ALK-positive NSCLC patients undergoing crizotinib treatment exhibit brain metastasis as the first site of disease progression, and in nearly 80% of these patients systemic disease is under control (Camidge, 2013; Solomon et al., 2014b). The physicochemical properties of PF-06463922 were specifically optimized to maximize its CNS availability. PF- 06463922 demonstrated 21% to 31% free brain drug exposure relative to free plasma concentration in non-tumor bearing rats and dogs, and is predicted to penetrate the intact bloodbrain barrier (BBB) in humans (Johnson et al., 2014).

To investigate the antitumor efficacy of PF-06463922 in a NSCLC brain metastasis model, we conducted intracranial xenograft studies with EML4-ALK-positive tumor models containing either wild-type EML4-ALK (H3122 or MGH006 cells) or the ALK^{L1196M} gatekeeper mutation (H3122 EML4-ALK^{L1196M} cells). Tumor cells were engineered to express either firefly luciferase or gaussia luciferase (Gluc) in order to allow noninvasive monitoring of tumor growth in vivo by either whole-body in vivo imaging systems (IVIS) or tail-vein blood Gluc activity measurement, respectively.

As shown by either MRI (Fig. 5A,B), IVIS (Fig. S5A–C) images, or blood Gluc activity measurements over time (Fig. 5C), PF-06463922 demonstrated significant antitumor activity against H3122 EML4-ALK^{WT} brain metastases that was superior to either crizotinib or alectinib. In subcutaneous studies, H3122 (EML4-ALK^{wt}) tumors displayed similar sensitivity to PF- 06463922 and alectinib (Fig.S4A). However, while H3122 brain metastases relapsed between 40 and 120 days after alectinib initiation, PF-06463922 treatment suppressed tumor growth in all mice for the duration of the experiment (160 days). Interestingly, shifting the alectinib-relapsed mice to PF-06463922 induced a second tumor response in those animals, demonstrating that PF-06463922 has superior intracranial efficacy compared with alectinib (Fig. 5C). The suppression in brain metastasis growth by PF-06463922 was consistent with better suppression of ALK phosphorylation (Fig. 5D). Immunohistochemistry (IHC) analysis indicated a significant reduction in the Ki67-positive tumor cell number and mitotic index in brain xenografts from mice within the 10 mg/kg/day BID treatment group (Fig. S5C, S5D).

Consistent with the H3122 EML4-ALK^{WT} brain metastasis study, PF-06463922 dose-dependently regressed H3122 EML4-ALK^{L1196M} brain metastases at 5, 10 and 20 mg/kg/day, corresponding to median free brain drug concentrations of 35, 55 and 100 ng/g respectively (Fig. S5E and F). In contrast, control-treated mice were euthanized, on average, 11 days after treatment initiation due to declining health attributed to tumor burden.

We hypothesized the superior inhibition of brain metastasis growth, attributed to better ALK kinase inhibition, was due to two factors – the enhanced potency of PF-06463922 and/or its increased ability to cross the BBB. To determine which mechanism attributed to its efficacy in our brain metastasis model, we tested an ALK inhibitor, PF-06439015, that possesses 1.5-fold greater potency than PF-06463922 but has poor CNS penetration (Huang et al., 2014; Johnson et al., 2014). Continued subcutaneous infusion of PF-06463922 (6–12 mg/kg/day) suppressed brain tumor growth better than PF-06439015 (36 mg/kg/day) (Fig. S5B). PK

analysis from these studies indicated that the brain free fraction of PF-06463922 (0.30 ± 0.13) relative to free plasma concentration was > 4-fold higher than that of PF-06439015 (0.07 ± 0.02) in mice bearing intracranial tumors. Similarly, better growth delay in the H3122 EML4-ALK^{L1196M} brain metastasis model was attributed to better drug penetration, as PF-06439015 failed to control their growth as brain tumor drug concentrations only reached 9.5 ng/g (Fig. S5E and F).

Patient-derived MGH006 cells expressing Gluc were equally sensitive to crizotinib and PF-06463922 in subcutaneous studies (Fig. S4F). When grown in the brain, however, PF-06463922 suppressed MGH006 tumor growth longer than crizotinib, leading to a significant improvement in survival (Fig. 5E and F). Crizotinib delayed MGH006 brain metastasis growth roughly 3-fold compared with control-treated mice, however all mice were euthanized within 45 days after treatment initiation due to neurological defects consistent with large CNS tumors. At this time point, brain metastases from PF-06463922-treated mice were barely detectable, and much smaller than when treatment was initiated. Consistent with their effects on brain metastasis growth, PF-06463922 achieved better suppression of ALK phosphorylation compared with crizotinib (Fig. 5G). Furthermore, we observed a reduction in total ALK levels in both treatment groups, but particularly after treatment with PF-06463922. It has been previously reported that HSP90 binding to ALK-fusion proteins in cells is disrupted by crizotinib treatment (Taipale et al., 2013). This disruption may contribute to the reduction in total ALK-fusion protein levels.

PF-06463922 demonstrated a broad therapeutic window in preclinical studies

PF-06463922 demonstrated antitumor efficacy in both subcutaneous and brain orthotopic xenograft models harboring oncogenic ALK fusions containing either wild-type ALK or crizotinib-resistant ALK mutants at pharmacologically relevant doses. PF-06469322 was well tolerated in mice (lack of significant weight loss) at all doses used in our studies (Fig.S6). This safety profile is also reflected by in vitro cell assays. For example, compared with other ALK inhibitors, PF-06463922 demonstrated superior activity against ALK-fusion transformed Ba/F3 cells compared with other ALK inhibitors (Table S1), while displaying less toxicity to parental Ba/F3 cells (IC_{50} >10 μM) (Fig. 6A). This finding is likely due to its high level of selectivity (Johnson et al., 2014).

The lack of toxicity of PF-06463922 in Ba/F3 cells, in combination with its superior potency, suggests that this compound could achieve a strong preclinical safety margin. The preclinical safety profile of PF-06463922 was characterized through single- and repeat-dose studies of up to 1 month in duration in rats and dogs, as well as safety pharmacology and genetic toxicity studies. The nonclinical safety findings related to PF-06463922 were identified at reasonable exposure margins above the efficacious concentration, and represent toxicities that can be monitored and are reversible following a one month treatment free period in rat and dog studies. PF-06463922 achieved a greater than 100-fold therapeutic index when comparing its Ceff (tumor stasis) in the EML4-ALK subcutaneous tumor growth model to its maximal tolerated dose (MTD) in both rats and dogs. The Ceffs derived from our in vivo studies are summarized in Table S4. It is worth mentioning that PF-06463922 achieved a maximal effect for either ALK target inhibition or tumor

regression in each of the tested efficacy models at exposure levels that are well below the MTD generated from one-month dog or rat safety studies (Fig. 6B). Since PF-06463922 is a brain penetrable compound, the potential for adverse CNS effects were tested in repeated dose safety studies as well as in the rat contextual renewal model. No CNS-mediated signals were observed in these studies. Furthermore, the functional observation battery (FOB) assessment was included in the one-month repeated dose study in the rat (data not shown). FOB is a series of noninvasive observational and interactive measures of CNS and automatic system function (e.g., body temperature, pupil response, gait, locomotor activity). No FOB effects were identified, despite achieving plasma exposures 60-fold higher than the predicted minimal efficacious exposure in humans (51 nM free), defined as the free compound concentration needed to achieve tumor stasis in the H3122 EML4-ALK^{L1196M} model.

DISCUSSION

The discovery of oncogenic ALK fusions and the development of ALK targeted therapies, like crizotinib, have transformed the course of disease for patients with ALK-driven cancers, particularly those with NSCLC. Patients derive significant benefit from either crizotinib or second-generation inhibitors alectinib or ceritinib. However, the majority of patients invariably relapse, and limited treatment options remain after relapse.

Here we report preclinical data on PF-06463922, a next generation ALK inhibitor that is currently in a Phase I/II clinical trial (NCT01970865) for ALK or ROS1 fusion-positive NSCLC. In a variety of different ALK inhibitor resistant models, PF-06463922 demonstrated broad activity across ALK resistant mutations, including G1202R that is the most refractory mutation identified to date. G1202R has rarely been reported in the setting of crizotinib resistance, but is emerging as a common resistant mutation to the 2nd generation ALK inhibitors ceritinib (Friboulet et al., 2014) or alectinib (Ignatius Ou et al., 2014). This is consistent with our preclinical studies showing that G1202R confers broad resistance to 1st and 2nd generation ALK inhibitors.

Although crizotinib has shown clinical activity against brain metastases, the CNS is a common site of relapse for patients on crizotinib (Costa et al., 2013; Costa et al., 2015; Solomon et al., 2014a; Solomon et al., 2014c). Mechanisms of resistance in the CNS to crizotinib have not been studied in detail, but one plausible mechanism is the inability of crizotinib to achieve therapeutic concentrations in the CNS compartment. Consistent with this notion, a case report showed low levels of crizotinib in the cerebrospinal fluid of a patient who had relapsed with brain metastases (Costa et al., 2011). Poor brain penetration of crizotinib is likely due to its high efflux by Pglycoprotein (PGP) (Johnson et al., 2014). Second generation ALK inhibitors have shown moderate CNS activity, including patients who have relapsed on crizotinib (Gadgeel et al., 2014). Similar to crizotinib, ceritinib is a PGP substrate and has limited brain penetration (Shaw et al., 2014b), and therefore responses to ceritinib likely reflect its increased potency. Alectinib, on the other hand, is not a PGP substrate and is associated with an intracranial response rate of 52% (Gadgeel et al., 2014). Nevertheless, patients treated with either ceritinib or alectinib still relapse with brain metastases, highlighting the need for a more potent inhibitor with increased CNS availability that, ideally, is not a substrate for PGP. PF-06463922 was specifically designed and

optimized to efficiently penetrate the BBB, and as a result it showed ~30% CNS availability in multiple preclinical species. We successfully mimicked the clinical situation in mouse models, and showed that ALK fusion tumors, sensitive to crizotinib when growing subQ, were resistant when growing in the brain parenchyma. Furthermore, PF-06463922 demonstrated superior efficacy to after alectinib relapse in our murine models of brain metastasis. PF- 06463922 regressed intracranial tumors at doses much lower than the MTD in our preclinical studies. In contrast, a potent ALK inhibitor with low CNS availability (6%) failed to sustain tumor growth inhibition in the same intracranial tumor model, suggesting penetration into the brain metastasis plays a major role in the activity of PF-06463922. While PF-06463922 provides hope that it will overcome brain metastases that develop in patients who relapse to 1st and 2nd generation ALK inhibitors, data from the ongoing Phase 1 study of PF-06463922 will be necessary to evaluate the CNS activity of PF-06463922 in humans, as preclinical studies may not predict brain penetration in humans.

The potency and safety profile, in combination with the penetration into the CNS, of PF-06463922 provides an opportunity to address both acquired and pharmacological mechanisms of drug resistance. Preclinical studies suggest a favorable preclinical safety window for PF-06463922 consistent with the ability to treat patients with drug exposures high enough to inhibit the most recalcitrant G1202R mutant and to reach therapeutic levels in the CNS. Preclinical studies are not always capable of predicting clinical toxicity, so data from the ongoing Phase 1 study of PF-06463922 will be critical in understanding the safety margin that PF-06463922 can achieve in humans.

The most immediate impact of PF-06463922 may be on patients that have failed previous ALK TKIs, not only in systemic disease but also with brain metastases. Given that PF-06463922 is the most potent and brain penetrable inhibitor that we tested in our models, whether it should be used as frontline treatment is an intriguing question that awaits clinical investigation. For example, could the frontline use of PF-06463922 lead to more durable responses than sequential therapy in the clinic, as suggested by the sustained responses seen with PF-06463922 in preclinical studies? Finally, if the safety and efficacy of PF-06463922 are confirmed in the clinic, PF-06463922 may serve as an ideal backbone for combination therapies aimed at overcoming and even preventing the emergence of resistant clones.

EXPERIMENTAL PROCEDURES

Enzyme Assays and compounds

Recombinant human wild-type and mutant ALK kinase domain proteins (amino acids 1093-1411) were produced in house using baculoviral expression, pre-activated via auto-phosphorylation with MgATP, and assayed for kinase activity using a microfluidic mobility shift assay. The reactions contained 1.3 nM wild-type ALK or 0.2–10 nM mutant ALK (appropriate to produce 15–20% phosphorylation of peptide substrate after 1-h reaction), 3 μM 5-FAM-KKSRGDYMTMQIG-CONH2, 5 mM $MgCl_2$ and the Km-level of ATP in 25 mM Hepes, pH 7.1. The Ki values were calculated by fitting the % conversion to a competitive inhibition equation (GraphPad Prism, GraphPad Software, San Diego, CA). PF-06463922 and PF-06439015 were synthesized as described in Huang, Q. 2014 (Huang et al., 2014) and Johnson, T., 2014 (Johnson et al., 2014), respectively; PF-02341066 as

described in Cui, J. 2011 (Cui et al., 2011). The physical properties of PF-06463922 were specifically optimized to maximize CNS availability by controlling molecular weight, lipophilicity, and hydrogen bond donor (HBD) count.

Cell Culture and Reagents

NCI-H3122 human NSCLC cells were licensed from National Institute of Health (NIH) (Rockville, MD). Karpas299 and NIH-3T3 cells were purchased from American Tissue Culture Corporation (ATCC) (Manassas, VA). BaF3 cells were obtained from DSMZ (Germany). NCIH3122 and NCI-H2228 are human lung adenocarcinoma cell lines harboring the EML4-ALK fusion protein variant 1 (V1) and variant 3 (V3a/b), respectively. The SNU2535, MGH056-1 and MGH021-5 NSCLC cell lines were derived from crizotinib, alectinib or ceritinib-relapsed patients and harbor the mutant ALK fusion proteins G1269A, G1202R or I1171T, respectively. MGH006, MGH051-1, MGH021-5 and MGH056-1 were maintained as previously described (Friboulet et al., 2014; Katayama et al., 2014; Katayama et al., 2012; Kim et al., 2013). Cell culture reagents were obtained from Life Technologies, Inc. Cells were maintained at 37°C in a humidified atmosphere with 5–10% CO2.

Engineered Cell Line Generation

The target of interest was first cloned into the retroviral vector pMSCV puro or pMSCVhygro. The retroviruses carrying recombinant genes were produced in 293T cells by co-transfection with the pMSCV vectors and the packaging plasmid pCL10A1. The retroviral supernatants were used to transduce NCI-H3122, NIH3T3 or BaF3 parental cells and pooled populations were selected with 2 g/ml puromycin or 50 g/ml hygromycin for 5 days.

Cell Based Kinase Phosphorylation ELISA Assays

Cells were seeded in 96-well plates in growth media with 0.5% serum and incubated overnight. Compounds were diluted in media without serum, added to the cells, incubated for one hour, and then removed by aspirating the media by vacuum suction. Cell lysates were generated and the phospho-ALK (Tyr1604) levels were determined by using the PathScan® Phospho-ALK (Tyr1604) Chemiluminescent Sandwich ELISA Kit (Cell Signaling, Cat#: 7020) or PathScan® Total ALK Chemiluminescent Sandwich ELISA Kit (Cell Signaling, Cat#: 7084) as described in the manufacturer's protocol. The IC_{50} values were calculated by concentration-response curve fitting utilizing a four-parameter analytical method. This phospho-ALK ELISA assay was also used to determine phosphor-ALK levels in the protein extracts from xenograft tumor samples.

Cell Proliferation Assay

Cells were seeded in 96-well plates in growth media containing 10% FBS and cultured overnight at 37°C. The following day, serial dilutions of PF-06463922 or appropriate controls were added to the designated wells, and cells were incubated at 37°C for 72 hours. A Cell Titer Glo assay (Promega, Madison, WI) was then performed to determine the relative cell numbers. IC50 values were calculated by concentration-response curve fitting utilizing a four-parameter analytical method.

Cell Caspase 3/7 Activity Assay

Cells were seeded in 96-well plates at 15,000 cells/well in RPMI media supplemented with 0.5% FBS (Assay Media) and allowed to adhere overnight at 37°C. The following day, 10mM PF- 06463922 was serially diluted in DMSO, and the DMSO dilutions were further diluted in Assay Media and added to the designated wells resulting in a range of serially diluted concentrations of PF-06463922 in the media with 0.5% serum and 0.1% DMSO. The cells were incubated for 24 hours, and the Caspase3/7 activity was measured using the Caspase-Glo® 3/7 Assay kit (Promega) as described in the manufacturer's protocol. The IC50 values were calculated by concentration-response curve fitting utilizing a four-parameter analytical method.

Animals

5–8 weeks old female nu/nu mice were obtained from Charles River (Wilmington, MA). Animals were maintained under clean room conditions in sterile filter top cages with Alpha-Dri bedding and housed on HEPA-filtered ventilated racks. Animals received sterile rodent chow and water ad libitum. All animal procedures were performed in compliance with the Institute for Laboratory Animal Research Guide for the Care and Use of Laboratory Animals and the Public Health Service Policy on Human Care of Laboratory Animals. Experiments were approved by the Animal Care and Use Committee at Pfizer La Jolla and by the Institutional Animal Care and Use Committee of Massachusetts General Hospital.

Drug administration

In all the tumor xenograft studies, the compound of interest was administered either orally at 5 to 10 mL/kg utilizing the sterile 20G feeding needles (popper and sons, inc., NY) or via a subcutaneous Alzet mini-pump (DURECT Corporation, Cupertino, CA) infusion.

Subcutaneous tumor model

The cells were supplemented with 50% Matrigel (BD Biosciences, San Jose CA) to facilitate tumor take. Cells (5×10^6 in 100 uL) were implanted subcutaneously (S.C.) into the hind flank region of the mouse and allowed to grow to the designated size prior to the administration of compound for each experiment. Tumor size was determined by measurement with an electronic calipers and tumor volume was calculated as the product of its length × width^2 × 0.4.

Intracranial tumor model

For injection into the brain, the head of the mouse was fixed with a stereotactic apparatus and the skull over the left hemisphere of the brain was exposed via skin incision. Using a high-speed air-turbine drill (CH4201S; Champion Dental Products) with a burr tip size of 0.5 mm in diameter, three sides of a square (2.5 mm in length, each side) were drilled through the skull until a bone flap became loose. Using blunt tweezers, the bone flap was pulled back, exposing the brain parenchyma. 100,000 cancer cells, diluted in 1 μL PBS, were stereotactically injected into the left frontal lobe of the mice. The bone flap was then placed back into position in the skull and sealed using histocompatible cyanoacrylate glue, and the skin atop the skull was sutured closed. Brain metastatic tumor growth was measured

through the use of Gaussia luciferase (Gluc), an in vivo secreted reporter expressed by tumor cells and measured in the peripheral blood. In similar models, the blood Gluc activity directly correlated with tumor volume (Kodack et al., 2012).

MRI study

MRI images were acquired with a Bruker 7.0T scanner with an Avance II console using a 72 mm ID linear birdcage resonator for transmission and a two element surface coil array for local reception. Pre- and post-contrast T1 weighted fast spin echo images were acquired. While in the scanner, the temperature and respiratory trace of each mouse monitored continuously. The isoflurane/oxygen mixture (1.4–2.0%) was adjusted based on the respiratory rate. The mouse temperature was stabilized by forced air heating with automatic feedback from a rectal temperature probe. Prior to post-contrast scans, mice were injected with gadolinium. Injections were timed such image acquisition coincided with a period of stable tumor contrast as determined in a pilot study. Tumor volume was calculated by manual segmentation of T1 weighted images using imageJ software.

Ex Vivo Target Modulation (PK/PD) Studies

For tissue and plasma processing for PK/PD studies, mice were humanely euthanized, blood and brain tissue samples were collected for PK analysis, and tumors were resected for PD analysis. Plasma and brain samples were analyzed for PF-06463922 concentration using LCMS analysis. Resected tumors were snap frozen and pulverized on a liquid nitrogen cooled cryomortar and pestle, and lysed in cold 1X Cell Lysis Buffer (Cell Signaling Technologies, Boston MT). Proteins were extracted from tumor lysate and protein concentrations were determined using a BSA assay (Pierce, Rockford, IL). The level of phosphorylated ALK in each tumor sample was determined using the capture ELISA or Western blotting methods.

Immunoblotting

Immunoblotting method was also used to determine relative kinase phosphorylation status and total protein levels in cells and tumor tissues for the protein of interest. Extracted protein samples from cells or tumor lysates were separated by SDS-PAGE, transferred to nylon membranes, and immunoblotting hybridizations for the proteins of the interest were performed using the corresponding antibodies. Phospho-ERK (T202/Y204), ERK, S6, phospho S6, phospho-AKT (S473 and T308), AKT, phospho-ALK (Y1282/1283), and ALK antibodies were obtained from Cell Signaling Technology. GAPDH was purchased from Millipore.

Statistics

Sample size for *in vivo* tumor growth inhibition (TGI) studies was estimated to be around n=8–12 per group to ensure a 80% power to capture 70% TGI in an 1-sided test based on variability estimate from historical data. Animals were randomized into different treatment groups stratified on their initial tumor size, so the average tumor size for each group is similar at baseline. Standard inclusion/exclusion criteria were used where animals are only excluded in rare occasions (such as death) after randomization. Investigators were not

blinded to treatment assignment. Due to skewed distribution of the tumor volume data, Analysis of Variance (ANOVA) models were fit to the rank transformed tumor volume. Individual comparisons between treatment groups and vehicle group or among the treatment groups were assessed with 1-sided LSD tests and, all under the ANOVA model for ranks.

Supplementary Material

Refer to Web version on PubMed Central for supplementary material.

ACKNOWLEDGEMENTS

This work was supported by a grant from the US National Institutes of Health (5R01CA164273-02 to A.T.S). The study was also supported by a grant from US Department of Defense Breast Cancer Research Innovator Award W81XWH-10-1-0016 and P01-CA080124 (to R.K.J.). Both L. E. and R. T. are now at Mirati Therapeutics, Inc., 9363 Towne Centre Drive, San Diego CA 92121.

REFERENCES

Bagrodia S, Smeal T, Abraham RT. Mechanisms of intrinsic and acquired resistance to kinase-targeted therapies. Pigment Cell Melanoma Res. 2012; 25:819–831. [PubMed: 22883054]

Camidge DR. Taking aim at ALK across the blood-brain barrier. J Thorac Oncol. 2013; 8:389–390. [PubMed: 23486263]

Camidge DR, Bang YJ, Kwak EL, Iafrate AJ, Varella-Garcia M, Fox SB, Riely GJ, Solomon B, Ou SH, Kim DW, et al. Activity and safety of crizotinib in patients with ALK-positive non-small-cell lung cancer: updated results from a phase 1 study. Lancet Oncol. 2012; 13:1011–1019. [PubMed: 22954507]

Chen J, Jiang C, Wang S. LDK378: a promising anaplastic lymphoma kinase (ALK) inhibitor. J Med Chem. 2013; 56:5673–5674. [PubMed: 23837797]

Choi YL, Soda M, Yamashita Y, Ueno T, Takashima J, Nakajima T, Yatabe Y, Takeuchi K, Hamada T, Haruta H, et al. EML4-ALK mutations in lung cancer that confer resistance to ALK inhibitors. N Engl J Med. 2010; 363:1734–1739. [PubMed: 20979473]

Costa DB, Kobayashi S, Pandya SS, Yeo WL, Shen Z, Tan W, Wilner KD. CSF concentration of the anaplastic lymphoma kinase inhibitor crizotinib. J Clin Oncol. 2011; 29:e443–e445. [PubMed: 21422405]

Costa DB, Shaw AT, I Ou S-H, Solomon BJ, Riely GJ, Ahn M-J, Zhou C, Shreeve SM, Wiltshire R, Selaru P, et al. MO07.02 Clinical Experience with crizotinib in patients with advanced ALK-rearranged non-small cell lung cancer and brain metastasis in profile 1005 and profile 1007. J. of Thoracic Oncology. 2013:S494–S495.

Costa DB, Shaw AT, Ou SH, Solomon BJ, Riely GJ, Ahn MJ, Zhou C, Shreeve SM, Selaru P, Polli A, et al. Clinical Experience With Crizotinib in Patients With Advanced ALK-Rearranged Non- Small-Cell Lung Cancer and Brain Metastases. Journal of clinical oncology : official journal of the American Society of Clinical Oncology. 2015

Crystal AS, Shaw AT, Sequist LV, Friboulet L, Niederst MJ, Lockerman EL, Frias RL, Gainor JF, Amzallag A, Greninger P, et al. Patient-derived models of acquired resistance can identify effective drug combinations for cancer. Science. 2014

Cui JJ, Tran-Dube M, Shen H, Nambu M, Kung PP, Pairish M, Jia L, Meng J, Funk L, Botrous I, et al. Structure based drug design of crizotinib (PF-02341066), a potent and selective dual inhibitor of mesenchymal-epithelial transition factor (c-MET) kinase and anaplastic lymphoma kinase (ALK). Journal of medicinal chemistry. 2011; 54:6342–6363. [PubMed: 21812414]

Doebele RC, Pilling AB, Aisner DL, Kutateladze TG, Le AT, Weickhardt AJ, Kondo KL, Linderman DJ, Heasley LE, Franklin WA, et al. Mechanisms of resistance to crizotinib in patients with ALK gene rearranged non-small cell lung cancer. Clin Cancer Res. 2012; 18:1472–1482. [PubMed: 22235099]

Friboulet L, Li N, Katayama R, Lee CC, Gainor JF, Crystal AS, Michellys PY, Awad MM, Yanagitani N, Kim S, et al. The ALK inhibitor ceritinib overcomes crizotinib resistance in non-small cell lung cancer. Cancer Discov. 2014; 4:662–673. [PubMed: 24675041]

Gadgeel SM, Gandhi L, Riely GJ, Chiappori AA, West HL, Azada MC, Morcos PN, Lee RM, Garcia L, Yu L, et al. Safety and activity of alectinib against systemic disease and brain metastases in patients with crizotinib-resistant ALK-rearranged non-small-cell lung cancer (AF-002JG): results from the dosefinding portion of a phase 1/2 study. Lancet Oncol. 2014; 15:1119–1128. [PubMed: 25153538]

Gainor JF, Shaw AT. Emerging paradigms in the development of resistance to tyrosine kinase inhibitors in lung cancer. J Clin Oncol. 2013; 31:3987–3996. [PubMed: 24101047]

Gandhi L, Drappatz J, Ramaiya NH, Otterson GA. High-dose pemetrexed in combination with high-dose crizotinib for the treatment of refractory CNS metastases in ALK-rearranged non-small-cell lung cancer. J Thorac Oncol. 2013; 8:e3–e5. [PubMed: 23242445]

Gerber DE, Minna JD. ALK inhibition for non-small cell lung cancer: from discovery to therapy in record time. Cancer Cell. 2010; 18:548–551. [PubMed: 21156280]

Huang Q, Johnson TW, Bailey S, Brooun A, Bunker KD, Burke BJ, Collins MR, Cook AS, Cui JJ, Dack KN, et al. Design of potent and selective inhibitors to overcome clinical anaplastic lymphoma kinase mutations resistant to crizotinib. J Med Chem. 2014; 57:1170–1187. [PubMed: 24432909]

Ignatius Ou SH, Azada M, Hsiang DJ, Herman JM, Kain TS, Siwak-Tapp C, Casey C, He J, Ali SM, Klempner SJ, Miller VA. Next-generation sequencing reveals a Novel NSCLC ALK F1174V mutation and confirms ALK G1202R mutation confers high-level resistance to alectinib (CH5424802/RO5424802) in ALK-rearranged NSCLC patients who progressed on crizotinib. J Thorac Oncol. 2014; 9:549–553. [PubMed: 24736079]

Johnson TW, Richardson PF, Bailey S, Brooun A, Burke BJ, Collins MR, Cui JJ, Deal JG, Deng YL, Dinh D, et al. Discovery of (10R)-7-amino-12-fluoro-2,10,16-trimethyl-15-oxo-10,15,16,17-tetrahydro-2H-8,4-(m etheno)pyrazolo[4,3-h][2,5,11]-benzoxadiazacyclotetradecine-3-carbonitrile (PF-06463922), a macrocyclic inhibitor of anaplastic lymphoma kinase (ALK) and c-ros oncogene 1 (ROS1) with preclinical brain exposure and broad-spectrum potency against ALK-resistant mutations. J Med Chem. 2014; 57:4720–4744. [PubMed: 24819116]

Kaneda H, Okamoto I, Nakagawa K. Rapid response of brain metastasis to crizotinib in a patient with ALK rearrangement-positive non-small-cell lung cancer. J Thorac Oncol. 2013; 8:e32–e33. [PubMed: 23486271]

Katayama R, Friboulet L, Koike S, Lockerman EL, Khan TM, Gainor JF, Iafrate AJ, Takeuchi K, Taiji M, Okuno Y, et al. Two novel ALK mutations mediate acquired resistance to the next-generation ALK inhibitor alectinib. Clinical cancer research : an official journal of the American Association for Cancer Research. 2014; 20:5686–5696. [PubMed: 25228534]

Katayama R, Khan TM, Benes C, Lifshits E, Ebi H, Rivera VM, Shakespeare WC, Iafrate AJ, Engelman JA, Shaw AT. Therapeutic strategies to overcome crizotinib resistance in non-small cell lung cancers harboring the fusion oncogene EML4-ALK. Proc Natl Acad Sci U S A. 2011; 108:7535–7540. [PubMed: 21502504]

Katayama R, Shaw AT, Khan TM, Mino-Kenudson M, Solomon BJ, Halmos B, Jessop NA, Wain JC, Yeo AT, Benes C, et al. Mechanisms of acquired crizotinib resistance in ALK-rearranged lung Cancers. Sci Transl Med. 2012; 4:120ra117.

Kim S, Kim TM, Kim DW, Go H, Keam B, Lee SH, Ku JL, Chung DH, Heo DS. Heterogeneity of genetic changes associated with acquired crizotinib resistance in ALK-rearranged lung cancer. J Thorac Oncol. 2013; 8:415–422. [PubMed: 23344087]

Kinoshita K, Asoh K, Furuichi N, Ito T, Kawada H, Hara S, Ohwada J, Miyagi T, Kobayashi T, Takanashi K, et al. Design and synthesis of a highly selective, orally active and potent anaplastic lymphoma kinase inhibitor (CH5424802). Bioorg Med Chem. 2012; 20:1271–1280. [PubMed: 22225917]

Kinoshita Y, Koga Y, Sakamoto A, Hidaka K. Long-lasting response to crizotinib in brain metastases due to EML4-ALK-rearranged non-small-cell lung cancer. BMJ Case Rep. 2013 *2013*.

Kodack DP, Chung E, Yamashita H, Incio J, Duyverman AM, Song Y, Farrar CT, Huang Y, Ager E, Kamoun W, et al. Combined targeting of HER2 and VEGFR2 for effective treatment of HER2-

amplified breast cancer brain metastases. Proceedings of the National Academy of Sciences of the United States of America. 2012; 109:E3119–E3127. [PubMed: 23071298]

Kwak EL, Bang YJ, Camidge DR, Shaw AT, Solomon B, Maki RG, Ou SH, Dezube BJ, Janne PA, Costa DB, et al. Anaplastic lymphoma kinase inhibition in non-small-cell lung cancer. N Engl J Med. 2010; 363:1693–1703. [PubMed: 20979469]

Lackner MR, Wilson TR, Settleman J. Mechanisms of acquired resistance to targeted cancer therapies. Future Oncol. 2012; 8:999–1014. [PubMed: 22894672]

Lovly CM, McDonald NT, Chen H, Ortiz-Cuaran S, Heukamp LC, Yan Y, Florin A, Ozretic L, Lim D, Wang L, et al. Rationale for co-targeting IGF-1R and ALK in ALK fusion-positive lung cancer. Nat Med. 2014; 20:1027–1034. [PubMed: 25173427]

Mager DE, Wyska E, Jusko WJ. Diversity of mechanism-based pharmacodynamic models. Drug Metab Dispos. 2003; 31:510–518. [PubMed: 12695336]

Maillet D, Martel-Lafay I, Arpin D, Perol M. Ineffectiveness of crizotinib on brain metastases in two cases of lung adenocarcinoma with EML4-ALK rearrangement. J Thorac Oncol. 2013; 8:e30–e31. [PubMed: 23486270]

Rosenzweig SA. Acquired resistance to drugs targeting receptor tyrosine kinases. Biochem Pharmacol. 2012; 83:1041–1048. [PubMed: 22227013]

Sasaki T, Koivunen J, Ogino A, Yanagita M, Nikiforow S, Zheng W, Lathan C, Marcoux JP, Du J, Okuda K, et al. A novel ALK secondary mutation and EGFR signaling cause resistance to ALK kinase inhibitors. Cancer Res. 2011; 71:6051–6060. [PubMed: 21791641]

Shaw AT, Engelman JA. ALK in lung cancer: past, present, and future. J Clin Oncol. 2013; 31:1105–1111. [PubMed: 23401436]

Shaw AT, Kim DW, Mehra R, Tan DS, Felip E, Chow LQ, Camidge DR, Vansteenkiste J, Sharma S, De Pas T, et al. Ceritinib in ALK-rearranged non-small-cell lung cancer. N Engl J Med. 2014a; 370:1189–1197. [PubMed: 24670165]

Shaw AT, Kim DW, Nakagawa K, Seto T, Crino L, Ahn MJ, De Pas T, Besse B, Solomon BJ, Blackhall F, et al. Crizotinib versus chemotherapy in advanced ALK-positive lung cancer. N Engl J Med. 2013; 368:2385–2394. [PubMed: 23724913]

Shaw AT, Mehra R, Tan D, Felip E, Chow L, Camidge DR, Vansteenkiste J, Sharma S, De Pas T, Riely G, et al. 1293P - Evaluation of ceritinib-treated patients (pts) with anaplastic lymphoma kinase rearranged (ALK+) non-small cell lung cancer (NSCLC) and brain metastasis. Annals of Oncology. 2014b; 25(suppl_4):iv426.

Solomon B, Felip E, Blackhall F, Mok T, Kim D, Wu Y, Nakagawa K, Mekhail T, Paolini J, Usari T, et al. Overall and incranial (IC) efficacy results and time to symptom deterioration in PROFILE 1014: 1st line crizotinib vs. premetrexed-platinum chemotherapy (PPC) in pateints with advanced ALK-positive non-squamous non-smeall cell lung cancer (NSCLC). Annals of Oncology. 2014a; 25(suppl_4):iv426–iv470.

Solomon B, Wilner KD, Shaw AT. Current status of targeted therapy for anaplastic lymphoma kinase-rearranged non-small cell lung cancer. Clin Pharmacol Ther. 2014b; 95:15–23. [PubMed: 24091716]

Solomon BJ, Mok T, Kim DW, Wu YL, Nakagawa K, Mekhail T, Felip E, Cappuzzo F, Paolini J, Usari T, et al. First-Line Crizotinib versus Chemotherapy in ALK-Positive Lung Cancer. N Engl J Med. 2014c; 371:2167–2177. [PubMed: 25470694]

Taipale M, Krykbaeva I, Whitesell L, Santagata S, Zhang J, Liu Q, Gray NS, Lindquist S. Chaperones as thermodynamic sensors of drug-target interactions reveal kinase inhibitor specificities in living cells. Nature biotechnology. 2013; 31:630–637.

Takeda M, Okamoto I, Nakagawa K. Clinical impact of continued crizotinib administration after isolated central nervous system progression in patients with lung cancer positive for ALK rearrangement. J Thorac Oncol. 2013; 8:654–657. [PubMed: 23584297]

Tanizaki J, Okamoto I, Okabe T, Sakai K, Tanaka K, Hayashi H, Kaneda H, Takezawa K, Kuwata K, Yamaguchi H, et al. Activation of HER family signaling as a mechanism of acquired resistance to ALK inhibitors in EML4-ALK-positive non-small cell lung cancer. Clin Cancer Res. 2012; 18:6219–6226. [PubMed: 22843788]

Weickhardt AJ, Scheier B, Burke JM, Gan G, Lu X, Bunn PA Jr, Aisner DL, Gaspar LE, Kavanagh BD, Doebele RC, Camidge DR. Local ablative therapy of oligoprogressive disease prolongs disease control by tyrosine kinase inhibitors in oncogene-addicted non-small-cell lung cancer. J Thorac Oncol. 2012; 7:1807–1814. [PubMed: 23154552]

Weinstein IB. Cancer. Addiction to oncogenes--the Achilles heal of cancer. Science. 2002; 297:63–64. [PubMed: 12098689]

Yamazaki S, Lam JL, Zou HY, Wang H, Smeal T, Vicini P. Translational pharmacokineticpharmacodynamic modeling for an orally available novel inhibitor of anaplastic lymphoma kinase and c-Ros oncogene 1. J Pharmacol Exp Ther. 2014; 351:67–76. [PubMed: 25073473]

Zou HY, Li Q, Engstrom LD, West M, Appleman V, Wong KA, McTigue M, Deng YL, Liu W, Brooun A, et al. PF-06463922 is a potent and selective next-generation ROS1/ALK inhibitor capable of blocking crizotinib-resistant ROS1 mutations. Proc Natl Acad Sci USA. 2015

SIGNIFICANCE

Though the development of ALK inhibitors has changed the course of treatment in NSCLC patients, tumors invariably relapse. Here, we demonstrate the superior properties of the next generation ALK inhibitor PF-06463922 compared with clinically available ALK inhibitors. PF- 06463922 addresses two major mechanisms of clinical relapse, ALK resistance mutations and brain metastasis. Superior potency, selectivity and physicochemical properties of PF-06462922 are reflected in its ability to achieve potent inhibition of all tested ALK resistance mutations, to penetrate the CNS and regress brain metastasis, while having robust safety margins in preclinical studies. PF-06463922 has the potential to treat ALK-driven cancer in both the refractory setting as well as in the frontline setting.

A

Recombinant ALK kinase domain variant	PF-06463922 Ki GMean (GCI95)	
	nM	n
Wild-type	<0.07	5
L1196M	0.6 (0.5-0.9)	5
G1269A	0.9 (0.3-3.0)	2
1151Tins	0.1	1
G1202R	ND	
L1152R	<0.1	1
S1206Y	0.2	1
C1156Y	<0.1	1
F1174L	<0.1	1

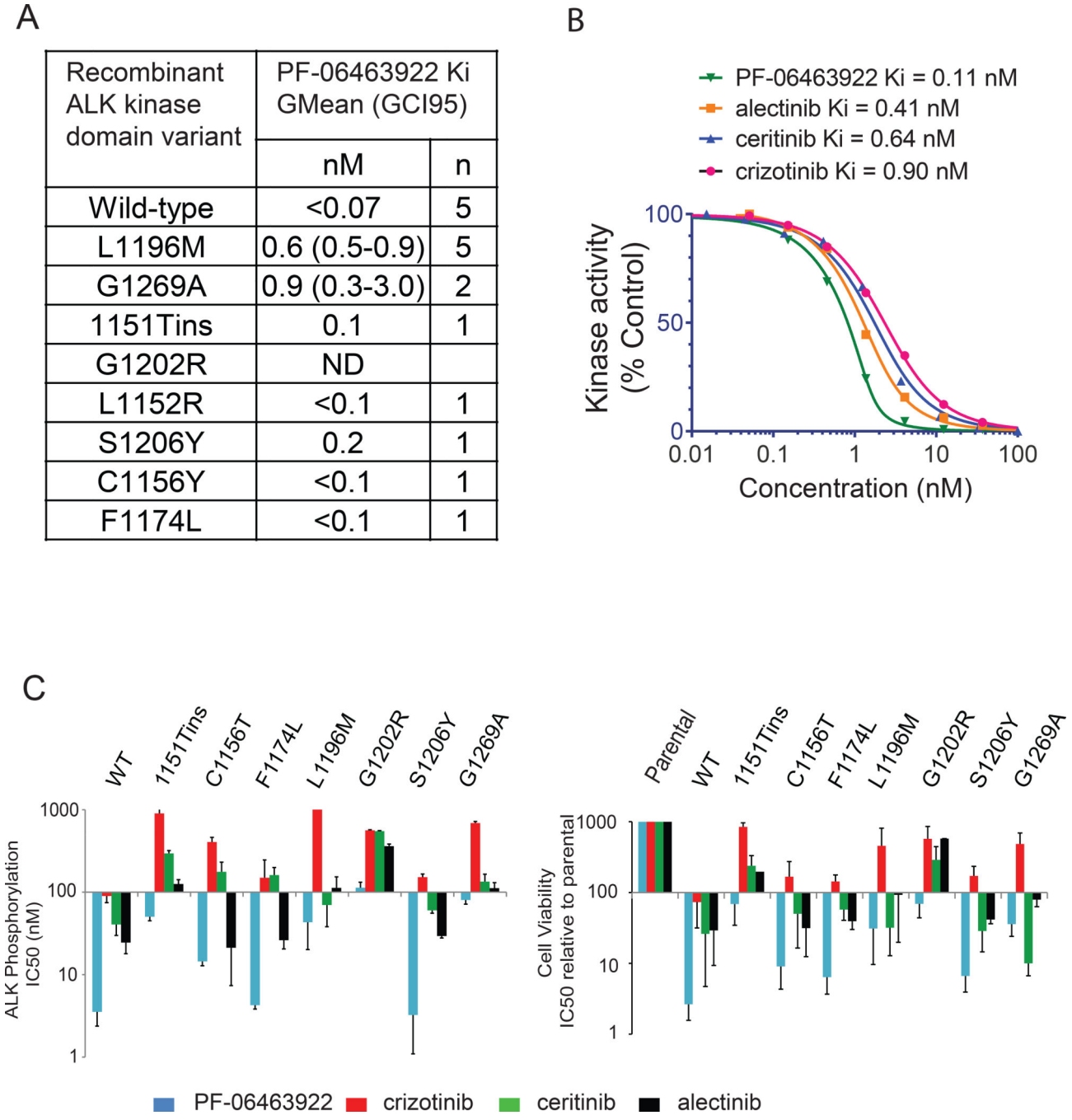

Figure 1. PF-06463922 is a potent inhibitor of wild-type ALK and crizotinib-resistant ALK mutants

A) PF-06463922 in biochemical kinase assays with the indicated recombinant ALK kinase domain constructs. Ki values are geometric means with a 95% confidence interval for n independent measurements. B) Biochemical kinase activity of recombinant human wild-type ALK kinase domain treated with the indicated concentrations of PF-06463922, crizotinib, ceritinib and alectinib. The kinase activity was assayed by a microfluidic mobility shift assay. **C)** IC_{50} of PF-06463922, crizotinib, ceritinib and alectinib on ALK phosphorylation (left panel) and cell viability (right panel) across different Ba/F3 cell lines expressing wild-

type or mutated EML4-ALK relative to parental IL-3–dependent Ba/F3 cells. Values are presented as mean +/− SD (n=3). See also Figure S1 and Table S1.

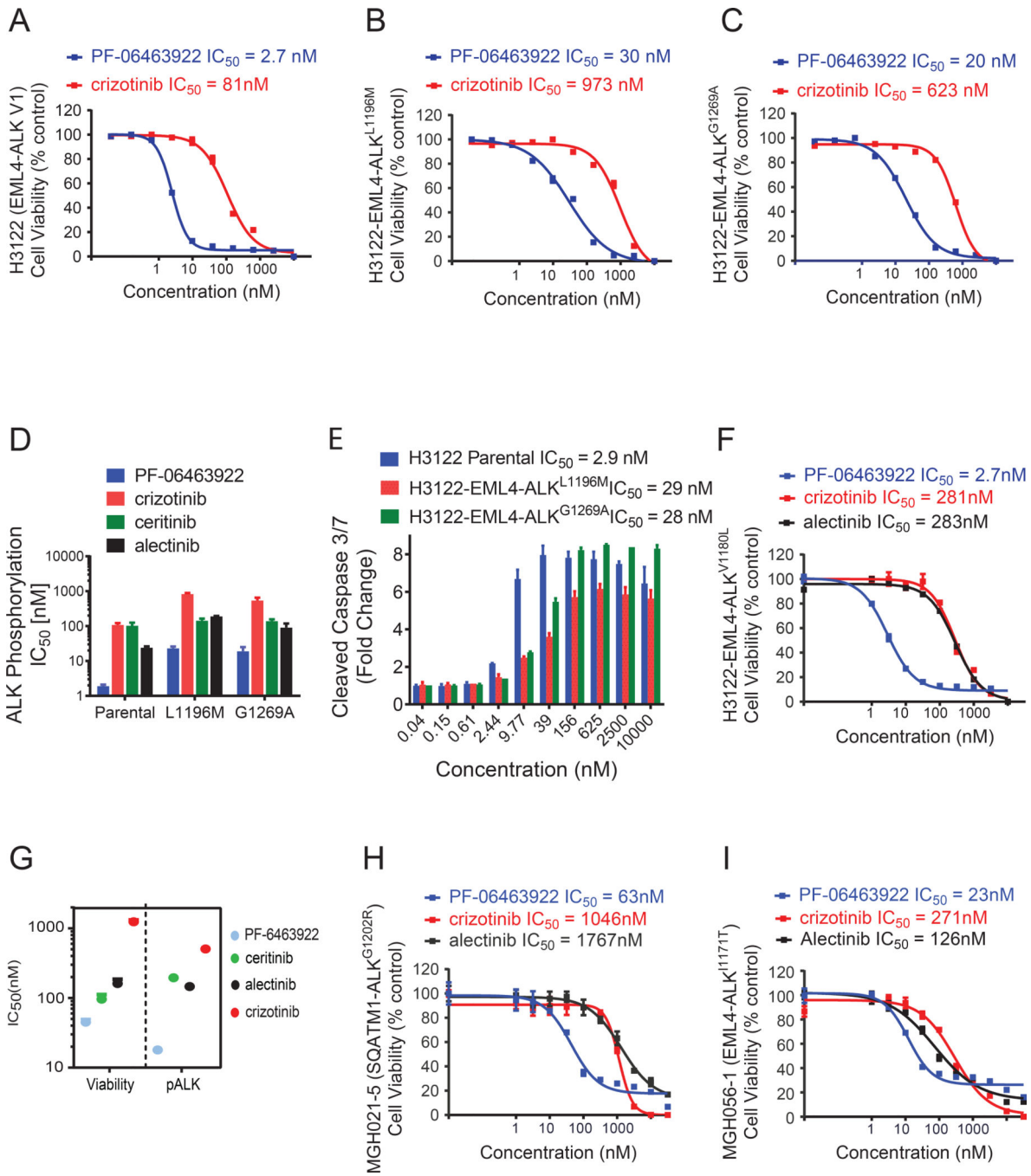

Figure 2. PF-06463922 potently inhibits ALK fusion wild type and mutant-mediated tumor cell survival

(A–C) Cell viability assays of H3122 EML4-ALK^{WT} (A), H3122 EML4- ALK^{L1196M} (B), H3122 EML4-ALK^{G1269A} (C) cells treated with the indicated doses of crizotinib or PF-06463922 for 72 hours. Cell viability was assayed by Cell-Titer-Glo. For panels A–C, values are presented as mean +/− SEM (n=3) D) IC_{50} of PF-06463922, crizotinib, ceritinib and alectinib on ALK phosphorylation in H3122 cell lines expressing EML4-ALK^{WT}, EML4-ALK^{L1196M} and EML4-ALK^{G1269A}. Values are presented as mean +/− SEM (n=3–

7). E) Cleaved caspase 3/7 induction by PF-06463922 treatment in the three different H3122 cell models. Values are presented as mean +/− SD (n=3). F) Cell viability assay of the alectinib-resistant H3122 cell line (EML4-ALK^{V1180L}) treated with the indicated doses of crizotinib, PF-06463922 or alectinib for 72 hours. Values are presented as mean +/− SEM (n=6) G) Cell survival and ALK phosphorylation IC50s of PF-06463922, crizotinib, ceritinib and alectinib on crizotinib-resistant patient-derived cell line SNU2535 (EML4-ALK^{G1269A}). Values are presented as mean +/− SEM (n=3–14). H) Cell viability assay of ceritinib-resistant patient-derived cell line MGH021-5 (SQSTM1-ALK^{G1202R}) treated with the indicated doses of crizotinib, PF-06463922 or alectinib for 7 days. I) Cell viability assay of alectinib-resistant patient-derived cell line MGH056-1 (EML4-ALK^{I1171T}) treated with the indicated doses of crizotinib, PF-06463922 or alectinib for 72 hours. For panels H and I values are presented as mean +/− SEM (n=3). See also Figure S2.

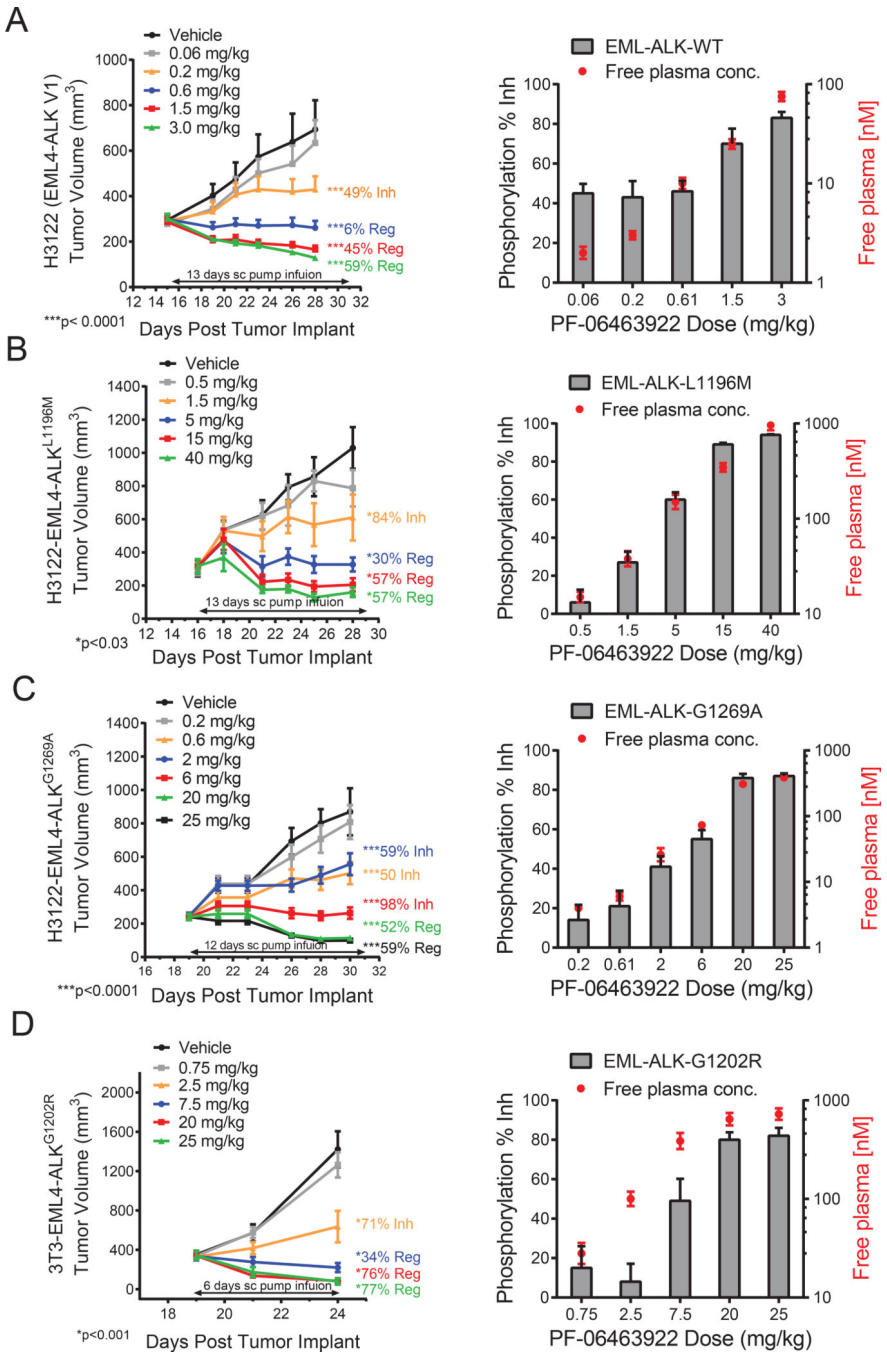

Figure 3. PF-06463922 ALK target inhibition PK/PD relationships in ALK fusion driven subcutaneous tumor xenograft models in mice

Mini-pump infusion study in H3122 model expressing endogenous EML4-ALK^{WT}(A), H3122 model expressing engineered EML4-ALK^{L1196M} (B), H3122 model expressing engineered human EML4-ALK^{G1269}(C), 3T3 model expressing engineered human EML4-ALK^{G1202R} (D). Tumor sizes (left) and pALK level and PF-06463922 free plasma concentration (right) of each group are indicated. ALK phosphorylation in tumors was measured at the time of sacrifice following the last tumor volume measurement. The tumors were collected and processed immediately after sacrifice. Tumor volumes, ALK

phosphorylation and plasma concentration values are presented as mean +/− SEM (n=8–12). See also Figure S3, Table S2, Table S3 and Table S4.

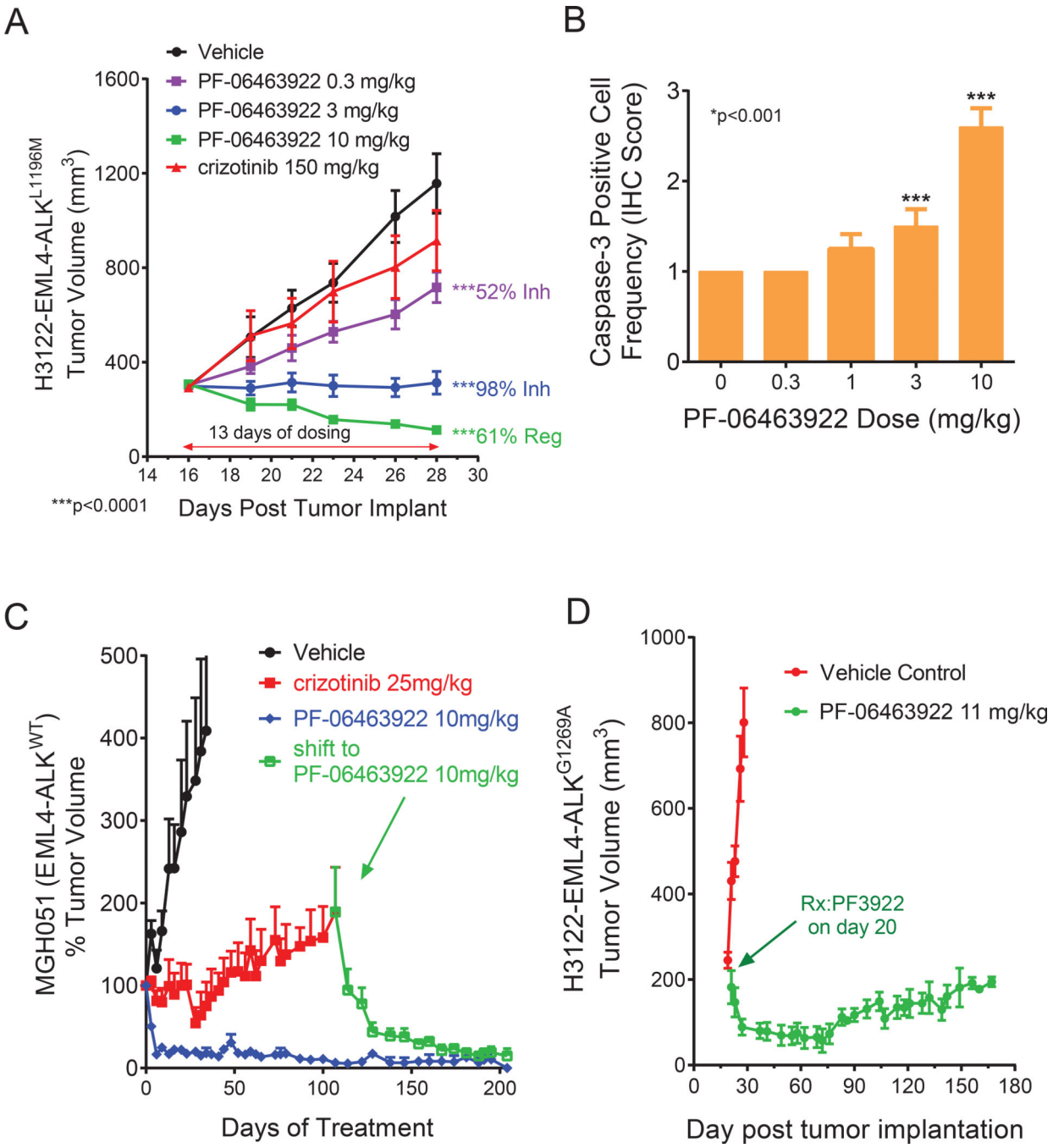

Figure 4. PF-06463922 antitumor efficacy in ALK fusion driven subcutaneous xenograft tumor models in mice

A) Subcutaneous tumor growth in the H3122 EML4-ALK^{L1196M} tumor model treated with orally dosed crizotinib 75 mg/kg BID or PF-06463922 0.3–10 mg/kg BID for 13 days. Tumor volumes are presented as mean +/− SEM (n=12). B) Activated-Caspase3 positive cell numbers following 3-day of oral BID administration of PF-06463922 in the H3122-EML4-ALK^{L1196M} model (cf. Fig. 4A). Values = Mean +/− SEM (n=7–9). C) Long term subcutaneous tumor growth in the EML4-ALK^{WT} MGH051 crizotinib-resistant patient-derived model treated with crizotinib 25 mg/kg QD or PF-06463922 10 mg/kg BID. The

mice treated with crizotinib were shifted to PF-06463922 after 107 days of treatment (arrow). Tumor volumes are presented as mean +/− SD (n=5–12). D) Long term subcutaneous tumor growth of the H3122-EML4-ALKG^{1269A} tumors treated with PF-06463922 subcutaneous pump infusion at 11 mg/kg/day for 172 days. Tumor volumes are presented as mean +/− SEM (n=5–12). See also Figure S4.

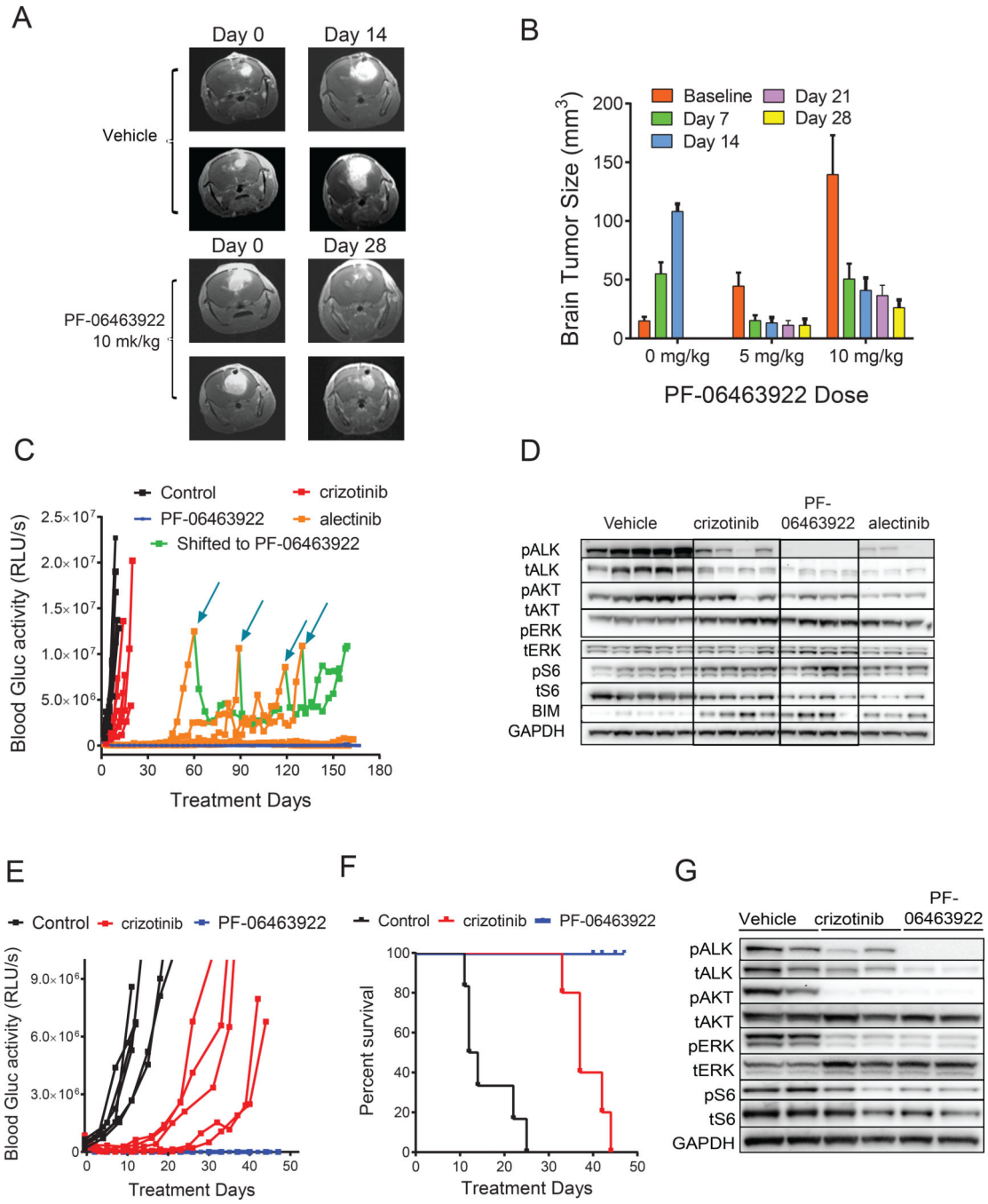

Figure 5. PF-06463922 antitumor efficacy in ALK fusion-driven intracranial tumor models

A) Representative MRI images showing regression of large established H3122 EML4-ALK^{WT} intracranial tumors in mice following PF-06463922 infusion. B) Quantitation of brain tumor sizes following PF-06463922 treatment in the H3122 EML4-ALK^{WT} intracranial model shown in panel A. Values are presented as mean +/− SEM. C) Oral dosing of PF-06463922, crizotinib and alectinib. Long term brain orthotopic tumor growth of H3122 EML4-ALK^{WT} cells expressing secreted luciferase treated with crizotinib 50 mg/kg QD or alectinib 60 mg/kg QD or PF-06463922 10 mg/kg BID. The mice treated with

alectinib were shifted to PF-06463922 at the indicated times (blue arrows). D) Pharmacodynamic analysis of H3122 EML4-ALK^{WT} brain tumors treated for 3 days and collected 3 hours after last treatment. (E,F) Brain tumor growth (E) and Kaplan-Meier survival curves ($p<0.0001$) (F) of MGH006 EML4-ALK^{WT} patient-derived cell line in mice treated orally dosed with crizotinib 100 mg/kg QD or PF-06463922 10 mg/kg/day BID for 42 days. G) Pharmacodynamic analysis of MGH006 brain tumors treated for 3 days and collected 3 hours after last treatment. Individual blood Gluc activity values are presented for each mouse (n=5–7 per group). See also Figure S5.

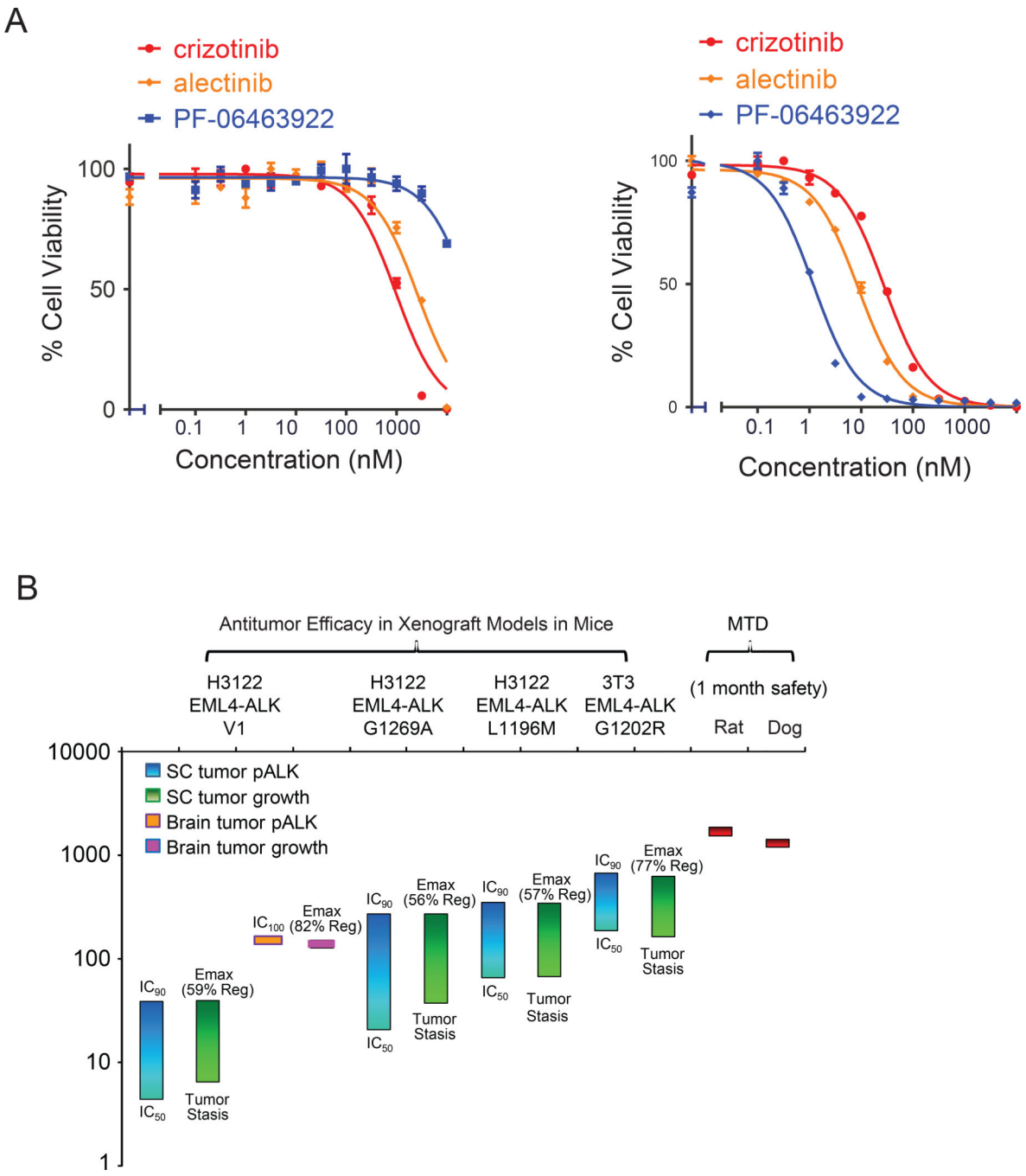

Figure 6. PF-06463922 preclinical pharmacology profile

A) Cell survival curves of Ba/F3 parental (left) or EML4-ALK^{WT} –expressing cells (right) following treatment for 48 hr with crizotinib, alectinib or PF-06463922. Cell survival was assayed using Cell-Titer-Glo. Values are presented as mean +/− SEM (n=3) B) PF-06463922 preclinical pharmacology profile and safety margin. See also Figure S6.